Journal of Solid State Chemistry **160,** 25–32 (2001)
doi:10.1006/jssc.2000.9142, available online at http://www.idealibrary.com on IDEAL®

The Structural Transformation from the Pyrochlore Structure, $A_2B_2O_7$, to the Fluorite Structure, AO_2, Studied by Raman Spectroscopy and Defect Chemistry Modeling

Marianne Glerup,*,[1] Ole Faurskov Nielsen,* and Finn Willy Poulsen†

** Department of Chemistry, University of Copenhagen, Universitetsparken 5, DK-2100 Copenhagen Ø, Denmark; and †Materials Research Department, Risø National Laboratory, Frederiksborgvej 399, DK-4000 Roskilde, Denmark*

Received November 9, 2000; in revised form March 7, 2001; accepted March 15, 2001; published online June 7, 2001

Pyrochlore oxides of the composition $Y_2Ti_{2-y}Zr_yO_7$, with $y = 0$, 0.3, 0.6, and 0.9, were studied using Raman spectroscopy. Doping with Zr^{+4}, a homovalent ion, gradually induces the material to undergo a structural change from the perfect pyrochlore structure to a defect pyrochlore structure and ends at an oxygen deficient fluorite structure with the formula $(Y, Ti, Zr)_1O_{1.75}$. Invoking the bigger Zr^{+4} ion on the Ti^{+4} site causes this structural transformation. We have also investigated highly Ti-doped YSZ ceramic samples, which all have an oxygen deficient cubic fluorite structure. These samples have formula units between $(Y, Ti, Zr)_1O_{1.675}$ and $(Y, Ti, Zr)_1O_{1.90}$. It is argued that a band observed at 750 cm^{-1} in both the Ti-doped pyrochlore samples and in the Ti, Y, Zr fluorite samples is due to oxygen in seven fold coordination around Ti. Local structures are accordingly observed by Raman in these samples. We finally report a Raman spectrum of orthorhombic Y_2TiO_5. A defect chemistry model has been formulated, which qualitatively describes the observed pyrochlore–fluorite structural transition.

INTRODUCTION

Perfect pyrochlore oxides, $A_2B_2O_7$, are cubic with two different types of oxygen ions. The A ion is coordinated to 8 oxygen atoms and the B ion is coordinated to 6 oxygen atoms. Neutron diffraction experiments on $Y_2Ti_{2-y}Zr_yO_7$ (1) has shown that when the Zr^{+4} concentration increases a third oxygen position will become occupied, corresponding to a defect pyrochlore structure. With $y = 0.9$ the oxide can be described as belonging to an oxygen defect cubic fluorite structure. The structural transformation is caused by the increase of the six-coordinated B-ion radius, $r(Ti^{+4}) = 0.605$ Å and $r(Zr^{+4}) = 0.72$ Å (2). Compounds with fluorite structures have the general formula AO_2, where the A ion is coordinated to 8 oxygen atoms. Cubic yttria-stabilized-zirconia (YSZ) materials with the fluorite structure have been studied for many years because of their application as an electrolyte for solid oxide fuel cells (SOFC) (3). In doped zirconias the average cation-oxygen coordination numbers are between 6 and 8. The highly doped Ti-YSZ oxides have also shown possibilities as an anode material for SOFC, because of the materials ability to act as a mixed conductor, i.e., an oxide ion conductor and electronic conductor (4, 9).

Cubic ZrO_2 and YSZ have in the $k = 0$ approximation only one allowed fundamental transition, F_{2g}, but in the Raman spectra of these compounds more bands are always observed (5, 16).

In this investigation we hope to increase the knowledge of the gradual structural transformation from a pyrochlore structure to the defect fluorite structure, and thus enhance our understanding of defect fluorite structures. To our knowledge it is the first time that Raman spectra of highly doped Ti-YSZ materials, the $Y_2Ti_{2-y}Zr_yO_7$ pyrochlores and Y_2TiO_5, are reported.

The complete ternary phase diagram for ZrO_2–$YO_{1.5}$–TiO_2 appears not to have been determined. We have tried to sketch a phase diagram in Fig. 1 from the published binary systems: ZrO_2–$YO_{1.5}$ (6) and TiO_2–ZrO_2 (7), and $YO_{1.5}$–TiO_2 (8) Also included in the figure are data from Kaiser *et al.* (9) on the composition range for cubic, fully stabilized zirconia with up to 20 mole% titania (shaded area). The broken lines indicate approximate limits for the solid solution ranges. The solid solution range around the pyrochlore composition $Y_2Ti_2O_7$ is only 2–3 mole% according to (8). The investigated compositions of the present work are marked by small filled squares and a star in Fig. 1. The composition $Y_{0.5}(Ti_{0.15}Zr_{0.35})O_{1.75}$ (marked with a star) lies well within the fluorite structure phase field, but also on the line for stoichiometric pyrochlore compositions starting

[1] To whom correspondence should be addressed. E-mail: marianne.glerup@risoe.dk.

0022-4596/01 $35.00

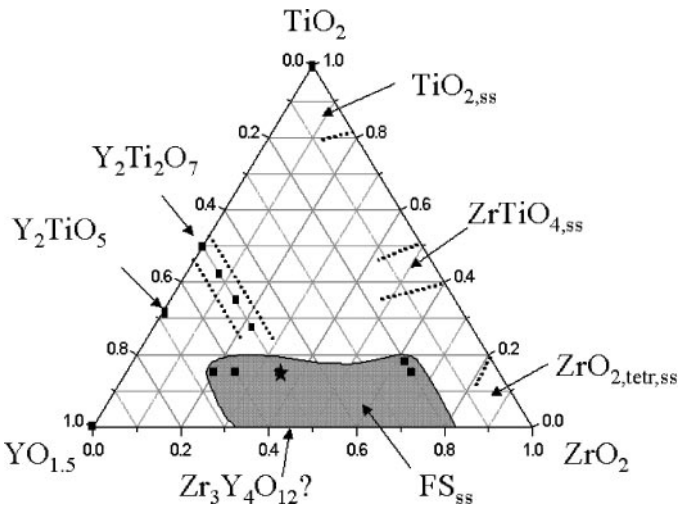

FIG. 1. Tentative ternary phase diagram for ZrO_2–$YO_{1.5}$–TiO_2 based on data in Refs. (6–9).

at $Y_2Ti_2O_7$. We initially asked ourselves the following crucial question: Will the Raman spectra of the pyrochlore series, moving from $Y_2Ti_2O_7$ toward the $Y_{0.5}(Ti_{0.15}Zr_{0.35})O_{1.75}$ composition gradually approach that of the disordered fluorite?

EXPERIMENTAL

Pyrochlore Materials

The ceramic samples were prepared by solid state synthesis (10). Ball milling was carried out of the oxides over night, followed by heating at 1400°C in air for 8 h. These procedures were repeated until single-phase materials were achieved. The following oxides were synthesized: $Y_2Ti_2O_7$, $Y_2Ti_{1.7}Zr_{0.3}O_7$, $Y_2Ti_{1.4}Zr_{0.6}O_7$, and $Y_2Ti_{1.1}Zr_{0.9}O_7$.

Fluorite Structures (Ti, Y) Doped ZrO_2

Preparation of the highly titania doped YSZ materials is described in Ref. (11) and the following compositions are investigated in this paper: $Y_{0.20}Ti_{0.15}Zr_{0.65}O_{1.90}$, $Y_{0.50}Ti_{0.15}Zr_{0.35}O_{1.75}$, $Y_{0.60}Ti_{0.15}Zr_{0.25}O_{1.70}$, and $Y_{0.65}Ti_{0.15}Zr_{0.20}O_{1.675}$.

Other Compositions

Y_2TiO_5 was made by solid state reaction between Y_2O_3 and TiO_2 at 1300°C, with three intermediate grindings and reheating. Laboratory grade (99.9%) rutile TiO_2 and cubic Y_2O_3 (Johnson–Matthey) were used.

X-Ray

X-ray powder diffraction was carried out on all the ceramic samples to check that the materials were single phase and to determine the lattice parameters. The X-ray diffraction experiments were done with white Cu radiation (1.2 kW) on a STOE θ–θ reflection diffractometer. An energy-dispersive Kevex detector was tuned to Cu$K\alpha$ (8.04 keV) with an energy window of 300 eV.

The structure analysis was carried out using the Rietveld program WinPLOTR (12).

NIR–FT–Raman

NIR–FT–Raman spectra were recorded on a Bruker model IFS 66 spectrometer equipped with a FRA 106 FT–Raman module using near infrared laser excitation (Nd : YAG, 1064 nm). A Ge detector, cooled to liquid nitrogen temperature, was used. All spectra were obtained in a 180° scattering configuration. The high-frequency detector cut-off was set at 3500 cm^{-1} (Raman shift), and a narrow band frequency filter removed the spectral features in the region from -100 to 84 cm^{-1} (Raman shifts). The laser output was 200 mW and the estimated spectral resolution was approximately 6 cm^{-1}.

VIS–Raman

The instrument used was a Dilor Z-24 Raman spectrometer equipped with a frequency-doubled Nd : YAG laser (532 nm). All spectra were measured in a 90° scattering configuration. Spectral width of 2.66 cm^{-1} and 200 mW laser power were used. All Raman spectra were recorded at room temperature.

RESULTS AND DISCUSSION

Phase Content

Unit cell parameters are given in Table 1, including fractional coordinates of the oxygens and occupancies for the four pyrochlore compositions obtained by Rietveld refinement. Vegard's law for the lattice parameter is perfectly obeyed. The trend in oxygen occupancy, as found in (1) could be confirmed by our X-ray data: the O(1) 48*f* position is gradually depopulated and the empty O(3) 8*b* position is being populated as the Zr content is increased, whereas the O(2) 8*a* position is kept fully populated. For the undoped pyrochlore, no refinement was made on the occupancies. For the doped compositions, the sum of the Zr and Ti was kept constant, but for the oxygen occupancies the refinement was done without restrictions, meaning that the sum of the oxygen content is not correct. A fully occupied position has by definition the occupancy = 1 in Table 1. The $\chi^2 = (R_{wp}/R_{exp})^2$ values for the fits in Table 1 were 3.1, 8.0, 6.1, and 16.0, respectively, for the compositions $y = 0$, 0.3, 0.6, and 0.9. The χ^2 values are rather large as expected for refinement on X-ray data obtained by a conventional powder diffractometer; however, the trends in both the

TABLE 1
Unit Cell Parameters for the Pyrochlore Samples

	$Y_2Ti_{2-y}Zr_yO_7$			
Site	$y = 0$	$y = 0.3$	$y = 0.6$	$y = 0.9$
a (Å)	10.0904 (0.0002)	10.1385 (0.0003)	10.1937 (0.0003)	10.2367 (0.0003)
Y ion 16*c* (0,0,0) Occupancy	1.0000	1.0000	1.0000	1.0000
Ti ion 16*d* ($\frac{1}{2},\frac{1}{2},\frac{1}{2}$) Occupancy	1.0000	0.8025 (0.0096)	0.6516 (0.0096)	0.4614 (0.0118)
Zr ion 16*d* ($\frac{1}{2},\frac{1}{2},\frac{1}{2}$) Occupancy	1.0000	0.1975 (0.0096)	0.3484 (0.0096)	0.5386 (0.0118)
O(1) ion 48*f* ($x,\frac{1}{8},\frac{1}{8}$) Occupancy	1.0000	0.9556 (0.0175)	0.9259 (0.0163)	0.9031 (0.0175)
Fractional coordinate, x	0.4231 (0.0009)	0.4189 (0.0006)	0.4151 (0.0006)	0.4100 (0.0008)
O(2) ion 8*a* ($\frac{1}{8},\frac{1}{8},\frac{1}{8}$) Occupancy	1.0000	0.9777 (0.0294)	0.9646 (0.0282)	1.0008 (0.0388)
O(3) ion 8*b* ($\frac{3}{8},\frac{3}{8},\frac{3}{8}$) Occupancy	0.0000	0.0492 (0.0236)	0.1303 (0.0233)	0.3189 (0.0357)

Note. The numbers in brackets are the standard deviations.

x coordinate and the occupancies were confirmed by starting with widely different starting values for these parameters.

The powder diffraction patterns of Y_2TiO_5 revealed that when cooled from 1300°C it has the orthorhombic structure described by Mumme and Wadsley (13) with 7-fold coordinated Y and 5-fold coordinated Ti. Samples cooled from 1550°C at ~100°C/h had very strong peaks from a high temperature disordered fluorite structure polymorph (7) with $a = 5.1496 \pm 0.0006$ Å, and only minor traces (<5%) of the low temperature phase were seen.

Factor Group Analysis and Expected Normal Modes

Cubic pyrochlores. Cubic pyrochlores, $A_2B_2O(1)_6O(2)$, belong to the space group ($Fd\bar{3}m$, O_h^7), no. 227, with $Z = 8$. The site symmetry is D_{3d} for A and B ions, C_{2v} for the O(1) ions, and T_d for the O(2) ion, which is in accordance with reference (14). Factor group analysis was made on the basis of the above site symmetries. The vibrational normal modes were predicted as follows, in accordance with (15)

$$\Gamma_{\text{opt.}}^{*2} = A_g^{(R)} + 3A_{2u}^{(i.a)} + E_g^{(R)} + 3E_u^{(i.a)} + 2F_{1g}^{(i.a)} + 7F_{1u}^{(IR)} + 4F_{2g}^{(R)} + 4F_{2u}^{(i.a)}$$

$$\Gamma_{\text{ac.}} = F_{1u}.$$

Raman active vibrations per set of ions were

A ion: *none*

B ion: *none*

O(1) ion: $A_g + E_g + 3F_{2g}$

O(2) ion: F_{2g}

Cubic fluorites. Cubic fluorites, AO_2, belong to the space group ($Fm\bar{3}m$, O_h^5), no. 225, where $Z = 4$. The site symmetry is O_h for the A ion and T_d for the O ion, the normal modes predicted are, in accordance with (16),

$$\Gamma_{\text{opt.}} = F_{1u}^{(IR)} + F_{2g}^{(R)}$$

$$\Gamma_{\text{ac.}} = F_{1u}$$

Raman active vibrations per set of ion are

A ion: *none*

O ion: F_{2g}.

Y_2TiO_5. Y_2TiO_5 belongs to the orthorhombic space group (*Pnma*, D_{2h}^{16}) no. 62 with $Z = 4$. The site symmetry is C_s for all the atoms: Y(1), Y(2), Ti(1), O(1), O(2), O(3), O(4), and O(5) according to (13).

The normal modes predicted are

$$\Gamma_{\text{opt.}} = 16A_g^{(R)} + 8A_u^{(i.a.)} + 8B_{1g}^{(R)} + 15B_{1u}^{(IR)} + 16B_{2g}^{(R)} + 7B_{2u}^{(IR)} + 8B_{3g}^{(R)} + 15B_{3u}^{(IR)}$$

$$\Gamma_{\text{ac.}} = B_{1u} + B_{2u} + B_{3u}.$$

Raman active vibrations per set of ion are

Y(1)-ion: $2A_g + B_{1g} + 2B_{2g} + B_{3g}$

and the same for the rest of the ions.

It is mentioned in Ref. (13) that Y_2TiO_5 could alternatively belong to the orthorhombic space group $Pn2_1a$, C_{2v}^9. The site symmetry for the ions would then be C_1 allowing all 93 normal modes to be active in the Raman spectrum. Since we only observe ~7 peaks in the spectrum we find it more likely that the low-temperature form of Y_2TiO_5 can be the more symmetric orthorhombic space group *Pnma*.

[2] (*) Denotes (R) Raman active, (IR) Infrared active, and (i.a.) inactive.

Reasons for Violation of the Selection Rules

More bands may be observed than predicted due to (i) a change of local symmetry or coordination numbers, e.g., from CN = 6 or 8 to CN = 5 or 7; (ii) a breakdown of the selection rules due to the presence of "foreign" atoms/ions allowing silent or IR-active modes to appear in the Raman spectrum, including combination tones with non-Raman active modes; (iii) allowance for $k \neq 0$ modes.

Gradual frequency changes, as the dopant level level is increased, may result from longer/shorter bond distances.

Spectra of Pyrochlore Samples

NIR–FT–Raman spectra of the undoped and doped pyrochlore oxides $Y_2Ti_2O_7$, $Y_2Ti_{1.7}Zr_{0.3}O_7$, $Y_2Ti_{1.4}Zr_{1.1}O_7$, $Y_2Ti_{1.1}Zr_{0.9}O_7$, and $Y_2Ti_{0.6}Zr_{1.4}O_7$ are shown in Fig. 2. The composition $Y_2Ti_{0.6}Zr_{1.4}O_7$ is more correctly described as a defect fluorite structure $(Y_{0.5}Ti_{0.15}Zr_{0.35})O_{2-0.5/2}$ and not as a pyrochlore structure. The above compositions are plotted in the same figure since they all lie on a straight line in the ternary phase diagram with the same oxygen content.

Raman frequencies for the undoped and doped pyrochlore oxides are shown in Table 2. The bands in the Raman spectra are tentatively assigned to symmetry species in Fig. 2 by comparing with previously published Raman spectra of pyrochlore oxides including $Y_2Ti_2O_7$ (17). The spectrum of single-crystal $Y_2Ti_2O_7$ in the I_{VV} geometry was shown Ref. (17), and therefore, the relative intensities are different from the intensities in the powder spectrum shown in the present work.

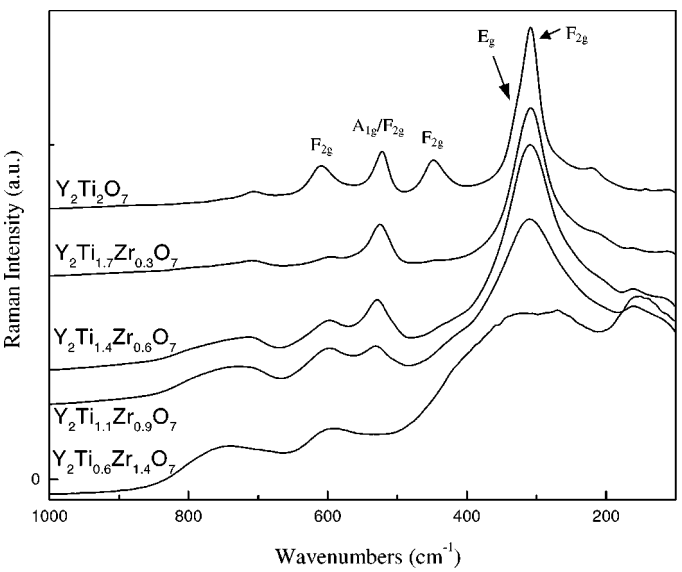

FIG. 2. NIR–FT–Raman spectra of the undoped and doped pyrochlore oxides: $Y_2Ti_2O_7$, $Y_2Ti_{1.7}Zr_{0.3}O_7$, $Y_2Ti_{1.4}Zr_{0.6}O_7$, $Y_2Ti_{1.1}Zr_{0.9}O_7$, and $Y_2Ti_{0.6}Zr_{1.4}O_7$.

TABLE 2
Observed Bands in the Raman Spectra for $Y_2Ti_{2-y}Zr_yO_7$

$Y_2Ti_2O_7$ (cm^{-1})	$Y_2Ti_{1.7}Zr_{0.3}O_7$ (cm^{-1})	$Y_2Ti_{1.4}Zr_{0.6}O_7$ (cm^{-1})	$Y_2Ti_{1.1}Zr_{0.9}O_7$ (cm^{-1})
221	~211	—	—
309	308	309	310
333	333	—	—
448	443	~420	~413
522	525	529	531
609	597	597	598
720	720	720	720
—	—	750	750

We can see from the factor group analysis made in this paper on pyrochlore structures that the cations do not contribute to the allowed fundamental transition, so doping with the Zr^{4+} ion on the *B* site will not directly influence the Raman spectra.

Although, it is observed that when Zr^{+4} is invoked in the structure, slight shifts of the vibrational frequencies are observed. Furthermore, the bands broaden and the peak intensities decrease.

In the Raman spectrum of the material with $y = 0.3$ the exact same peaks are observed as for the undoped pyrochlore oxide, but the $F_{2g} + A_{1g}$ band at $\sim 309\,cm^{-1}$ has broadened and the bands at 442 and $597\,cm^{-1}$ have lost intensity. These trends are continually observed as the dopant concentration is increased. When $y = 1.4$ (a fluorite material) it looks like the F_{2g} and A_{1g} bands have split.

The neutron diffraction experiments (1) have shown that the occupancy of the O(2) position is unchanged up to $y > 0.9$. It is the occupancy at the O(1) site that is changing when the O(3) positions start to be occupied. A new band appears at $750\,cm^{-1}$ as the dopant concentration reaches $y = 0.6$. It could look like a frequency shift of the $720\,cm^{-1}$ band, but when the doping concentration is increased to 0.9 it is evident that it is actually a new vibrational band, which is observed. The band at $720\,cm^{-1}$ is observed in all the Raman spectra presented in this work and has also been reported in undoped $Y_2Ti_2O_7$; it is assigned to be a combination band as was also argued in (17).

The broad band at $\sim 750\,cm^{-1}$ is therefore assigned to oxygen in a Ti–O_7 coordinated species. Although the average (*A* and *B*) cation–oxygen coordination number is 7 for all the compositions in the series, a shift occurs going from the perfect pyrochlore, where an equal amount of cations have, respectively, 6 and 8 coordination, in the case of disordered fluorites, where many—maybe not all cations—in reality have ~ 7 oxygen neighbors.

The band at $750\,cm^{-1}$ is also observed for the highly Ti-doped YSZ but not in YSZ itself, see next paragraph, and here it is observed that the intensity of the band depends on

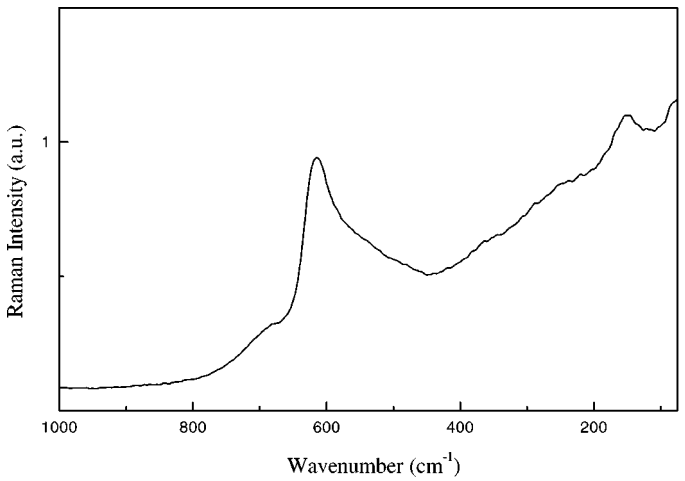

FIG. 3. NIR–FT–Raman spectrum of $Y_{0.18}Zr_{0.82}O_{1.91}$ (YSZ 10 mol%).

the Ti concentration. We conclude that the band is caused by a 1′ order vibrational transition and the reason for observing the band is that we observe local structures in the pyrochlore materials, which is in accordance with (15).

Fluorite Samples

Figure 3 shows the FT–Raman spectrum of a cubic 10 mol% yttria stabilized zirconia (10 mol% YSZ). The stoichiometric formula for this compound is $Y_{0.18}Zr_{0.82}O_{1.91}$. We observe no bands above 730 cm^{-1}, but also we observe more than the one allowed band predicted by factor group analysis. Figure 4 shows the VIS–Raman spectra of the highly doped Ti-YSZ samples. The composition $Y_{0.50}Zr_{0.35}Ti_{0.15}O_{1.75}$ was also shown in Fig. 2. A broad band with maximum at $\sim$745 cm^{-1} is observed. This is an additional proof for the 745 cm^{-1} bands belong to a Ti–O vibration. In these compounds, the cations have an average coordination to the oxygen on 7.6, 7.0, 6.8, and 6.7, respectively, going from high Zr content to low. The coordination number 7 corresponds directly to a disordered pyrochlore material.

The peak intensity at 620 cm^{-1} observed in the Raman spectra of Ti-YSZ and YSZ depends on the Zr^{+4} content, the band is very distinct when $Zr > 0.60$ w/w% but when $Zr \leq 0.35$ w/w% it is not well resolved. This band is also observed in the 10 mol% YSZ sample. At the same time, the intensity for the peak at $\sim$490 cm^{-1} assigned to the F_{2g} mode for cubic ZrO_2 (18) decreases or disappears with decreasing Zr^{+4}-content, and is therefore not easily observable.

Previous studies of the Raman spectra of Ti-doped 8 mol% YSZ by Traqueia *et al.* (19) showed that two local structures were present, e.g., cubic and tetragonal. This is understandable since the Y-concentrations are lower than in the present study. The coexistence of the two local structures however could not be observed using X-ray diffraction. The authors correlated the band at 720 cm^{-1} to depend on the Ti^{+4} concentration and assigned the band to a $Ti–O_6$ octahedral vibration.

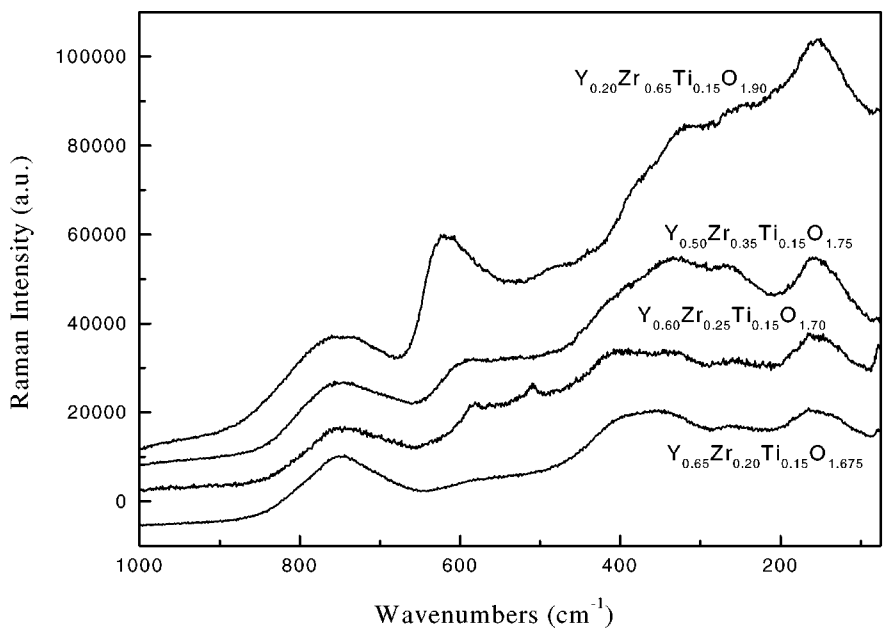

FIG. 4. VIS–Raman spectra of highly Ti-doped YSZ, e.g., $Y_{0.20}Ti_{0.15}Zr_{0.65}O_{1.90}$, $Y_{0.20}Ti_{0.18}Zr_{0.62}O_{1.90}$, $Y_{0.50}Ti_{0.15}Zr_{0.35}O_{1.75}$ (also shown in Fig. 2), $Y_{0.60}Ti_{0.15}Zr_{0.25}O_{1.70}$, $Y_{0.65}Ti_{0.15}Zr_{0.20}O_{1.675}$. The average oxygen coordination numbers are for the cations 7.6, 7.0, 6.8, and 6.7, respectively.

Spectrum of Y_2TiO_5

Pure orthorhombic Y_2TiO_5, was studied because it exhibits the unusual Ti–oxygen coordination number 5. In Fig. 5 we observe two high frequency modes at ≈ 860 and 730 cm^{-1}. In the five-fold coordination there is one quite short Ti–O bond of 1.78 Å and four longer bonds around 1.94 Å (13). Tentatively, we will assign the two peaks to strongly and less strongly bonded oxygen, respectively. The Ti–O separation in rutile is longer, 1.97 Å, resulting in an A_{1g} mode at 610 cm^{-1} (20). The Raman spectrum of Y_2TiO_5 cooled from 1550°C was very weak and had hardly any distinguishable peaks. This is in line with the X-ray data indicating that a supercooled disordered fluorite phase had been obtained.

Defect Chemistry Modeling of $Y_2Ti_{2-y}Zr_yO_7$ at Fixed pO_2

Below is described a first attempt to model an order–disorder transition by classical defect chemistry. The Kröger–Vink notation is used throughout (21). As seen in Table 3, the defect model is based on eight species. We assume that the model is valid for a pO_2 domain, where minor electronic defects, electron holes and electrons, and/or reduced cations, can be neglected. Also, in order to maintain simplicity, we assume that Ti always resides on the *B* site. We furthermore treat the two different oxygen sites in the pyrochlore structure, O(1) and O(2), as energetically equivalent. The O(3) on the 8*b* position will be modeled as interstitial oxygen, O_i''. The eight equations describing the interrelation between the eight concentrations are obtained

TABLE 3
Defect Model for a Pyrochlore with Simultaneous Disorder on the Cation and Oxygen Ion "Sublattices"

A site (16*c*)	*B* site (16*d*)	O sites (48*f*,8*a*)	O site (8*b*)
Y_A^x	Ti_B^x	O_O^x	O_i''
$Zr_A^{\bullet}$	Zr_B^x	$V_O^{\bullet\bullet}$	
	Y_B'		

Note. The site symmetries of the various sites are given as the Multiplicity and the Wykoff notation. The reference charges are + 3 for the *A* ion and + 4 for the *B* ion.

$$\text{A-site balance:}\quad [Y_A^x] + [Zr_A^{\bullet}] = 2 \qquad [1]$$

$$\text{B-site balance:}\quad [Zr_B^x] + [Ti_B^x] + [Y_B'] = 2 \qquad [2]$$

$$\text{O-site balance:}\quad [O_O^x] + [V_O^{\bullet\bullet}] = 7 \qquad [3]$$

$$\text{Mass balances:}\quad [Y_A^x] + [Y_B'] = 2 \qquad [4]$$

$$[Zr_B^x] + [Zr_A^{\bullet}] = y \qquad [5]$$

$$[Ti_B^x] = 2 - y \qquad [6]$$

Electroneutrality condition (EN):

$$[Zr_A^{\bullet}] + 2[V_O^{\bullet\bullet}] = 2[O_i''] + [Y_B']. \qquad [7]$$

The substitution of Ti by Zr is assumed to provoke disorder on the cation "sublattice" as well as a redistribution of oxygen between the "normal" sites in a pyrochlore structure and the vacant 8*b* positions. The defect model must therefore include a chemical equilibrium involving all

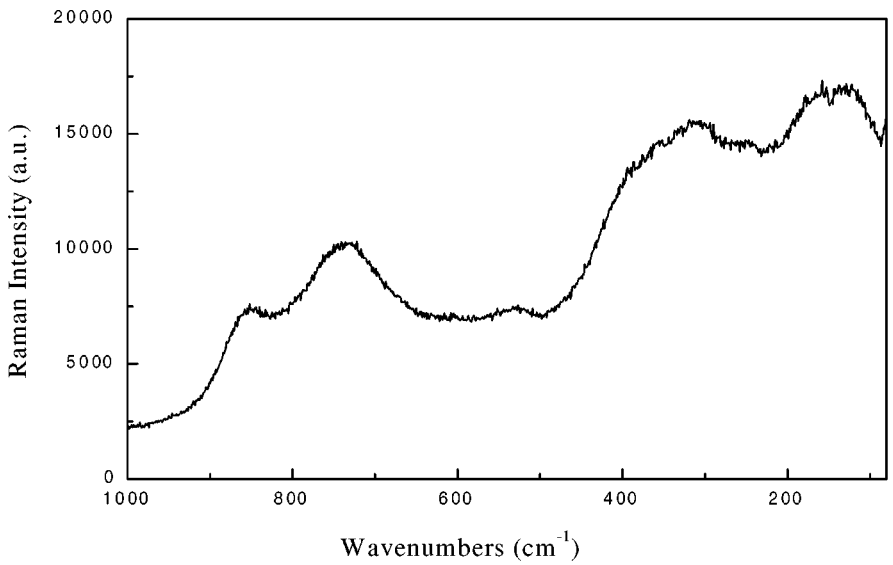

FIG. 5. VIS–Raman spectrum of the low-temperature orthorhombic form of Y_2TiO_5.

these species, i.e.,

$$Zr_B^x + Y_A^x + nO_O^x \Leftrightarrow Zr_A^\bullet + Y_B' + nV_O^{\bullet\bullet} + nO_i'' \qquad [8']$$

leading to the mass action law

$$K_{ex} = [Zr_A^\bullet] \bullet [Y_B'] \bullet [V_O^{\bullet\bullet}]^n \bullet [O_i'']^n / \{[Zr_B^x] \bullet [Y_A^x] \bullet [O_O^x]^n\}. \qquad [8'']$$

This mass law expression has been formulated for the general case, where n in principle can adopt both larger and smaller values than unity. In the following, we will only deal with the case $n = 7/8$. This choice leads to a statistical (complete) disorder on the cation and oxygen sites, respectively, for the hypothetical end member in the substitution series "$Y_2Zr_2O_7$" $= (Y/Zr)O_{1.75}$ (seven oxygens distributed on eight sites). It is in other words postulated that the (more complex) pyrochlore defect model can also describe the (simpler) case of a disordered fluorite. Using the linear mass-, site-, and electroneutrality equations [1–7], Eq. [8″] can be written as

$$K_{ex} = 64/49 \bullet [O_i'']^2 \, [O_i'']^{14/8} / \{(y - 8/7 \bullet [O_i'']) \bullet (2 - 8/7 \bullet [O_i'']) \bullet (7 - [O_i''])^{7/8}\}. \qquad [9]$$

The value of K_{ex}, leading to a statitical distribution, where $[O_i''] \equiv 7/8$, is then

$$K_{ex,\ y=2} = 1 \bullet 1 \bullet (7/8)^{7/8} \bullet (7/8)^{7/8} / \{1 \bullet 1 \bullet (49/8)^{7/8}\} = 0.1621. \qquad [10]$$

This value is close to the value of the anti-Frenkel constant,

$$K_{AF} = [O_i''] \, [V_O^{\bullet\bullet}] / [O_O^x] = 1/8, \qquad [11]$$

for a statistical distribution of the equilibrium $O_O^x \Leftrightarrow O_i'' + V_O^{\bullet\bullet}$ calculated in an earlier paper on the defect chemistry of the pyrochlore $Pr_2Zr_{1.6}Ce_{0.4}O_{7\pm\delta}$ (15). In the latter pyrochlore system there was only observed disorder on the oxygen "sublattice." For a known (or assumed) value of K_{ex}, one could choose to solve Eq. [9] for different values of the Zr-doping, y, by Newton–Raphson iteration. However, for the purpose of simulating the relationship

$$[O_i''] = f(y, K_{ex}), \qquad [12]$$

we can make the calculation much easier by inverting the problem to solve for the "inverse" relation

$$y = g([O_i''], K_{ex}). \qquad [13]$$

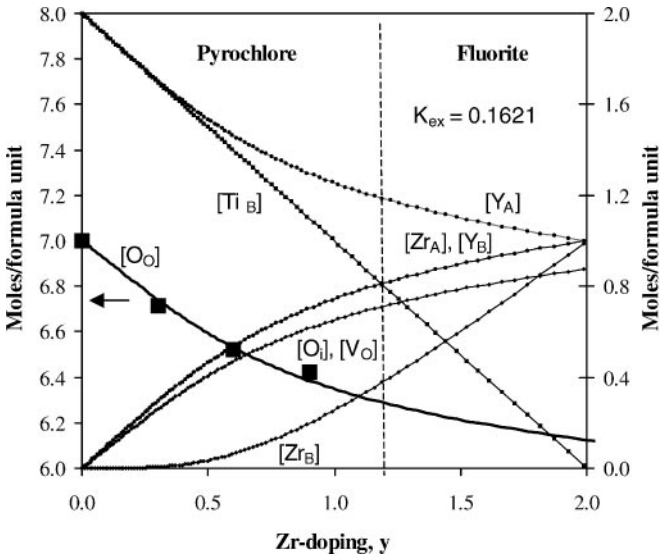

FIG. 6. Concentrations of defect species in pyrochlore $Y_2Ti_{2-y}Zr_yO_7$ at fixed pO_2. The equilibrium constant, $K_{ex} = 0.1621$, leads to complete disordering of oxygens and of Zr- and Y cations at the composition, $y = 2$. Kröger–Vink charges have been omitted in the figure. Filled symbols indicate the sum of oxygen on O(1) and O(2).

Rewriting Eq. [9] we find

$$y = 1/K_{ex} \bullet 64/49 \bullet [O_i'']^{30/8} / \{(2 - 8/7 \bullet [O_i'']) \bullet (7 - [O_i''])^{7/8}\} + 8/7 \bullet [O_i'']. \qquad [14]$$

Inserting values for $[O_i'']$ in the range $0 \le [O_i''] \le 7/8$ in Eq. [14] will deliver corresponding values of dopant levels, y. Figure 6 shows the distribution of ionic species as function of the doping level, using the statistical value for $K_{ex} = 0.1621$.

The approximate Zr-composition, $y \sim 1.2$, where the transition from pyrochlore to disordered fluorite structure occurs according to Kaiser *et al.* (9) has been marked by a vertical dashed line. Several features can be noticed from this calculation: (i) it is first observed that the concentration of the Zr-dopant on the A site, $[Zr_A^\bullet]$, rises much faster than the $[Zr_B^x]$ concentration; (ii) above $\approx y = 1.2$ most oxygen ions, which can be moved into the interstitial 8*b* position have done so; (iii) also passing $y = 1.2$, we come into a situation where there are more Y (originating from the A site) on the B site than Ti. All these trends are in line with the observed transition from an ordered pyrochlore to a disordered fluorite structure at a Zr-doping level around $y = 1.2$. Since the transition is a consequence of including the chemical equilibrium equation [8′] into the model, the transition must be gradual and not abrupt. This is qualitatively in agreement with the neutron study in (1), where

complete mixing of cations onsets at $y = 1.2$ and is complete at $y = 1.8$. Finally, the sum of oxygen on O(1) and O(2), according to the Rietveld refinement results in Table 1, is plotted for $y = 0$, 0.3, 0.6, and 0.9. We see that the model prediction mimics the oxygen occupancy found from X-ray quite well.

CONCLUSIONS

Raman spectroscopy shows a gradual change going from an ordered pyrochlore structure $Y_2Ti_2O_7$ to a disordered fluorite structure $Y_{0.5}(Ti_{0.15}Zr_{0.35})O_{1.75}$. A new Raman band, which cannot be predicted by conventional factor group analysis due to the disordered lattice, appears around 750 cm^{-1}, and was assigned to an increasing concentration of seven-coordinated Ti as the Zr doping level is increased. The band is absent in YSZ, which precludes that it could come from seven-coordinated Zr.

Defect chemistry modeling has succeeded qualitatively in rationalizing the smooth structural change.

ACKNOWLEDGMENTS

This study is part of the European TMR-project "Synthesis, Fabrication and Characterisation of Alternative Anodes for direct Methane Oxidation in SOFC's" (Contract FMRX-CT97-0130). Dr A. Kaiser is thanked for making the Ti-doped YSZ samples available to us. M.G. gratefully acknowledges the Danish Research Academy for funding. F.W.P. obtained financial support from the DK-SOFC programme. The Danish Natural Science Research Council and Haldor Topsøe A/S are thanked for funding the NIR–FT–Raman instrument within the Danish Materials Science Program.

REFERENCES

1. C. Heremans, B. J. Wuensch, J. K. Stalick, and E. Prince, *J. Solid State Chem.* **117,** 108–121 (1995).
2. R. D. Shannon, *Acta Cryst. A* **32,** 751–767 (1976).
3. S. P. S. Badwal, *Solid State Ionics* **52,** 23–32 (1992).
4. D. P. Fagg and J. T. S. Irvine, *Ionics* **4,** 61–71 (1998).
5. J. Cai, C. Raptis, Y. S. Raptis, and E Anastassakis, *Phys. Rev. B* **51,** 201–209 (1995).
6. H. G. J. Scott, *J. Mater. Sci.* **10,** 1527–1535 (1975).
7. A. V. Shevchenko, L. M. Lopato, I. M. Maister, and O. S. Gorbunov, Russ. *J. Inorg. Chem.* **25,** 1379–1381 (1980).
8. N. Mizutani, Y. Tajima, and M. J. Kato, *J. Am. Ceram. Soc.* **59,** 168 (1976).
9. A. Kaiser, A. J. Feighery, D. P. Fagg, and J. T. S. Irvine, *Ionics* **4,** 215–219 (1998).
10. P. Holtappels, F. W. Poulsen, and M. Mogensen, *Solid State Ionics* **135,** 675–679 (2000).
11. A. J. Feighery, J. T. S. Irvine, D. P. Fagg, and A. Kaiser, *Solid State Chem.* **143,** 273–276 (1999).
12. WinPLOTR, T. Roisnel, and J. Rodriguez-Carvajal, Laboratoire Léon Brillouin (CEA-CNRS), Beta version/Jan 99.
13. W. G. Mumme and A. D. Wadsley, *Acta Cryst. B* **24,** 1327–1333 (1968).
14. R. A. McCauley, *J. Appl. Phys.* **51,** 290–294 (1980).
15. F. W. Poulsen, M. Glerup, and P. Holtappels, *Solid State Ionics* **135,** 595–602 (2000).
16. N. Kjerulf-Jensen, R. W. Berg, and F. W. Poulsen, 2nd European Solid oxide fuel cell forum, proceedings, 6–18 May, 1996, Norway, Vol. 2, Edited by Bernt Thorstensen pp. 647–656.
17. M. T. Vandenborre, E. Husson, J. P. Chatry, and D. Michel, *J. Raman Spectrosc.* **14**(2), 63–71 (1983).
18. C. M. Phillippi and K. S. Mazdiyasni, *J. Am. Ceram. Soc.* **54,** 254–258 (1971).
19. L. S. M. Traqueia, T. Pagnier, and F. M. B. Marques, *Journal of the European Ceramic Society* **17,** 1019–1026 (1997).
20. M. Glerup, Ph.D. Thesis, University of Copenhagen (February, 2001).
21. F. A. Kröger, and H. J. Vink, *in* "Solid State Physics." (F. Seitz and D. Turnbull, Eds.), pp. 307–435, Academic Press In., New York, 1956.